

Resonant tunnelling through a C₆₀ molecular junction in a liquid environment

Lucia Grüter¹, Fuyong Cheng², Tero T Heikkilä¹,
M Teresa González¹, François Diederich²,
Christian Schönenberger¹ and Michel Calame¹

¹ Institut für Physik, Universität Basel, Klingelbergstraße 82, CH-4056 Basel, Switzerland

² Laboratorium für Organische Chemie, ETH-Hönggerberg, HCI, CH-8092 Zürich, Switzerland

E-mail: michel.calame@unibas.ch

Received 3 June 2005, in final form 15 July 2005

Published 9 August 2005

Online at stacks.iop.org/Nano/16/2143

Abstract

We present electronic transport measurements through thiolated C₆₀ molecules in a liquid environment. The molecules were placed within a mechanically controllable break junction using a single anchoring group per molecule. On varying the electrode separation of the C₆₀-modified junctions, we observed a peak in the conductance traces. The shape of the curves is strongly influenced by the environment of the junction as shown by measurements in two distinct solvents. In the framework of a simple resonant tunnelling model, we can extract the electronic tunnelling rates governing the transport properties of the junctions.

(Some figures in this article are in colour only in the electronic version)

1. Introduction

How can we experimentally determine the relevant energy levels and the tunnelling rates involved in electronic transport through single molecule devices? Such questions are of fundamental interest for the development of molecular electronics. The conductance of single molecules has been investigated in several experiments in which phenomena such as Coulomb blockade and Kondo effect [1, 2], negative differential resistance [3] and logic gates [4] were pointed out. Different techniques were used to address single or a few molecules. Fixed contact arrangements such as nanopore systems [5] and nanogaps fabricated by shadow evaporation or electromigration [6] have been realized. Alternatively, scanning tunnelling microscope (STM) [7, 8] and break-junction techniques [5, 9, 10] offer tunable contacts to characterize molecules. Break junctions offer an additional stability when compared to the STM, but the implementation of a third electrode remains delicate, although recent work shows that it can be done [11]. Adding a chemically controllable environment in break-junction experiments would provide

an additional control of the anchoring of the molecule to the metallic constriction and allow *in situ* electrochemistry experiments. The excellent efficiency of a liquid gate has been demonstrated previously on carbon nanotube field-effect transistors [12], and recently this effect has been studied for organic molecules using an STM [13, 14].

Buckminsterfullerenes and in particular C₆₀ and its derivatives have attracted much attention [15] and, due to their particular electronic properties, represent ideal model systems for molecular electronics [16–18]. In this paper, we present electronic transport measurements through thiolated C₆₀ derivatives in a two-probe configuration provided by the tips of a break junction (figure 1). The single functional group serves as an anchor and, in the case where a single molecule junction is realized, permits us to control the coupling of the C₆₀ to a gold electrode by mechanically adjusting the inter-electrode spacing *d*. By performing the transport measurements in two distinct solvents, dimethyl sulfoxide (DMSO) and toluene, we could observe the strong influence of the environment on the molecular junctions.

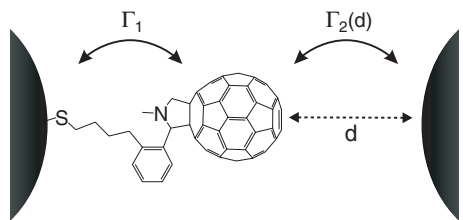


Figure 1. Schematic representation of a break junction with a thiolated C_{60} molecule anchored to the left electrode. The distance d between the molecule and the right electrode can be adjusted by opening and closing the junction.

2. Experimental section

The synthesis of the fullerene derivative was carried out following well-established protocols [19]. A thiolated C4 linker ensured that the C_{60} molecule would bind to the gold electrodes. To contact the molecules and perform transport measurements, we used a mechanically controllable break-junction setup [20]. A gold nanobridge was lithographically patterned on a phosphor bronze substrate. By bending the substrate via a vertically moving rod, the gold bridge is elongated and finally breaks. The two resulting ends serve as electrodes for contacting the molecules. The setup includes a cell that allows working in different liquid environments and has been described previously [21].

We first characterized the gold junctions via measurements of the conductance G versus distance d in air and in the solvents used subsequently for the C_{60} molecules, toluene and DMSO. Several sets of consecutive open–close cycles were recorded, with G ranging typically between $0.001G_0$ and a few G_0 , where $G_0 = 2e^2/h$ is the conductance quantum. To investigate the transport through C_{60} molecules, a 0.1 mM C_{60} solution was added to the liquid cell while the junction was kept closed. The junction was then opened widely (≈ 5 nm) to favour the self-assembly of the molecules. We also added molecules while keeping the junction open, but no significant differences in the transport measurements were observed. Sets of 10–30 $G(d)$ curves were recorded at time intervals of 30–45 min. During these cycles, the junction was never fully closed, keeping its conductance below $0.1G_0$ in order to limit the mechanical rearrangements of the Au tips. $G(d)$ -values obtained while closing the junction are shown in figure 2 for DMSO (a) and toluene (b) at a bias voltage of $V_b = 0.2$ V.

The open symbol curves show measurements in the pure solvent. The solid curves are five successive raw measurements performed after adding the C_{60} solution to the junction. We also attempted to measure current–voltage (I – V) characteristics. However, these curves were not reproducible, displaying rather large uncontrolled hysteresis, which we assign to the dynamics of the liquid environment and the relatively weak tethering of the C_{60} with one single linker group only.

While the measurements of $G(d)$ in the pure solvents show a clean exponential behaviour [21], the curves for the C_{60} modified junctions exhibit a more complex structure. In previous break-junction work with molecules, the occurrence of a plateau in $G(d)$ has been taken as the signature for the ‘locking-in’ of a molecule [10]. We observe a plateau in

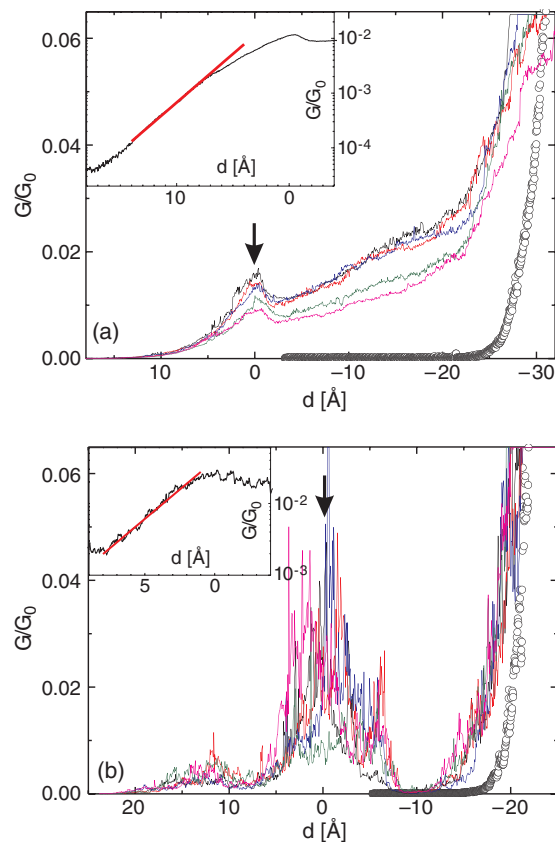


Figure 2. Conductance G versus distance d curves in DMSO (a) and toluene (b) measured at a bias voltage of 0.2 V while closing the junction. The open symbol curves were measured in the pure solvent. The solid lines are raw data for five successive measurements after adding the C_{60} solution. The insets show averaged (over ten curves) conductance data in a log–linear representation. The value for the inverse decay rate κ was obtained from a linear fit (solid lines) to G/G_0 in the low conductance regime: $\kappa_{\text{DMSO}} = 0.43 \text{ \AA}^{-1}$ and $\kappa_{\text{toluene}} = 0.37 \text{ \AA}^{-1}$. Note that the zero in the distance scale d was chosen to match with the position of the peak.

about 50% of the measured closing cycles. In addition to this observation, a pronounced peak can appear (arrows in figure 2). Although the peak appears less frequently in the different samples, reproducible measurements (visible in each closing curve within a cycle of ten curves at least) could be acquired for C_{60} in both DMSO and toluene. In DMSO, the peak corresponds to a conductance maximum of $\approx 0.012G_0$ and is followed by a plateau-like feature. On further closing the junction, the conductance rises more rapidly, although less sharply than in the pure solvent. The shape of the conductance curves in toluene (figure 2(b)) is very different, showing more noise and a fully developed peak. After a small pre-peak (not present in all curves), the conductance rises to a maximum value of $\approx 0.025G_0$ at the peak and decays again to a very low conductance. On further closing the junction, the conductance increases sharply, with a slope similar to that of the conductance in the pure solvent. The environment in which the junction is studied clearly plays an important role here. We note in particular that DMSO is a rather poor solvent for neutral fullerenes whereas toluene is a good one (see e.g. [22]).

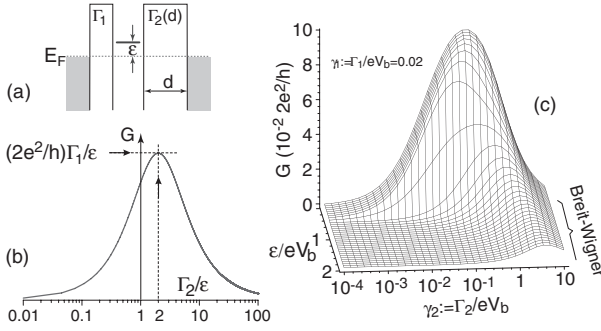


Figure 3. (a) Schematics of the energetics of a double-barrier junction with a single molecular level positioned at ε relative to the Fermi energy E_F of the metallic reservoirs. (b) Linear-response conductance G as a function of Γ_2 for the double-barrier shown in (a), assuming coherent tunnelling and $\Gamma_1 \ll \varepsilon$. (c) Same as (b), but taking into account the finite bias voltage $V_b \gg k_B T$. This illustration has been obtained for a specific value of $\Gamma_1 = 0.02V_b$. A pronounced crossover is observed at $\varepsilon = eV_b/2$.

To calibrate each junction, we measured the tunnelling conductance between the two Au electrodes in the pure solvent. Let us denote the gap distance between the two Au electrodes by d_{gap} . It can be expressed as $d_{\text{gap}} = rs$, where s denotes the vertical displacement of the pushing rod and r the reduction factor which depends on the geometry of the junction [20]. It is the reduction factor r which needs to be calibrated for each junction. The tunnelling conductance $G(s)$ measured in a pure solvent was fitted according to the expression $G(s) \propto \exp[-\kappa rs]$ with $\kappa = 2\sqrt{2m\phi}/\hbar$, where ϕ (and κ) represents the height of a square tunnelling barrier of width d_{gap} and m is the electron mass. The fits were adjusted by tuning r in order to obtain values for ϕ in agreement with our previous work [21] in which the apparent workfunctions in different solvents were calibrated with respect to measurements in vacuum. The reference inverse decay lengths κ , valid for the pure solvents, are $\kappa_{\text{toluene}} = 0.85 \text{ \AA}^{-1}$ and $\kappa_{\text{DMSO}} = 0.63 \text{ \AA}^{-1}$. This procedure provides the reduction factor r for each junction measured [23].

3. Discussion

The particularity of our system lies in the single anchor group used to tether the molecule within the break junction. This configuration makes it possible to tune the coupling of the molecule to the electrode: while one tunnelling rate (Γ_1/\hbar) is fixed, the second (Γ_2/\hbar) varies exponentially with the gap between the electrode (electrode to the right in figure 1) and the C₆₀ molecule. The metal–molecule–metal junction forms a double-barrier junction. In this picture, the observed conductance peaks can be explained within a coherent resonant tunnelling model, provided that one of the energy levels of the molecule lies not too far away from the Fermi level of the electrodes (figure 3(a)).

Resonant tunnelling through a single-level ε results in a peak in the linear conductance G when the level aligns with the Fermi level E_F of the leads, i.e. at $\varepsilon = 0$. The occurrence of a peak in $G(\varepsilon)$ is a well-known fact [24]. However, a peak can also arise in $G(\Gamma_2)$, even if $\varepsilon \neq 0$. Resonant tunnelling is

described by the Breit–Wigner equation:

$$G = \frac{2e^2}{h} \frac{\Gamma_1 \Gamma_2}{\varepsilon^2 + (\Gamma_1 + \Gamma_2)^2/4}. \quad (1)$$

In our geometry, Γ_1 is fixed and defined by the molecular tether holding the molecule to the left electrode (figure 1). Γ_2 depends exponentially on the distance d between the C₆₀ molecule and the right electrode, with κ being the inverse decay length, i.e. $\Gamma_2(d) = \Gamma_2^* e^{-\kappa d}$. $G(\Gamma_2)$ in equation (1) as a function of Γ_2 has a maximum G_{max} at $\Gamma_2^* = \sqrt{4\varepsilon^2 + \Gamma_1^2}$. For $\varepsilon \ll \Gamma_1$ we would have $\Gamma_2^* = \Gamma_1$ and consequently a peak conductance of $G_{\text{max}} \simeq G_0$. In the experiment, the peak conductance is however much smaller than G_0 , so $\Gamma_1 \ll \varepsilon$. It follows then that $\Gamma_2^* \simeq 2\varepsilon$ and $G_{\text{max}} = G_0 \Gamma_1/\varepsilon$. A respective plot in this limit ($\Gamma_1 \ll \varepsilon$) is shown in figure 3(b). Note that we define $\varepsilon \geq 0$, but the sign of ε is not determined, i.e. a sign change in ε does not affect the discussion.

Using the Breit–Wigner equation we can obtain the ratio Γ_1/ε from the measured peak height without fitting. The measurements yield $\Gamma_1/\varepsilon \simeq 1.1 \times 10^{-2}$ in DMSO and $\Gamma_1/\varepsilon \simeq 2.7 \times 10^{-2}$ in toluene, more than twice the DMSO value. Because we expect Γ_1 to be the same for both solvents (after all, it is the same linker), this suggests that the level is lying closer to the Fermi level of the electrodes in toluene as compared to DMSO.

That we can measure directly the ratio Γ_1/ε is a very nice fact. But we would like to obtain both ε and Γ_1 . This is at first sight not possible, because equation (1) is scale invariant. Changing Γ_1 , Γ_2 , and ε by the same factor leaves the curve invariant. To our rescue, we emphasize that we did not measure the linear-response conductance, but G at a bias of $V_b = 0.2 \text{ eV}$, much larger than $k_B T$ at room temperature. The finite bias introduces an energy scale which allows a considerable narrowing down of the range of possible values.

Integrating equation (1) over the bias window, given by the applied voltage V_b , yields

$$G = \frac{4e^2}{h} \frac{\gamma_1 \gamma_2(d)}{\gamma_1 + \gamma_2(d)} \left[\arctan\left(\frac{1 - 2\tilde{\varepsilon}}{\gamma_1 + \gamma_2(d)}\right) + \arctan\left(\frac{1 + 2\tilde{\varepsilon}}{\gamma_1 + \gamma_2(d)}\right) \right]. \quad (2)$$

All parameters are now scaled to V_b , i.e. $\gamma_i = \Gamma_i/eV_b$, $\gamma_2(d) = \gamma_2^* e^{-\kappa d}$, and $\tilde{\varepsilon} = \varepsilon/eV_b$. There are two regimes: (a) $\varepsilon \lesssim V_b/2$ and (b) $\varepsilon \gg V_b/2$; the latter corresponds to the Breit–Wigner equation. In both cases a peak develops in $G(\gamma_2)$, but there is a pronounced crossover, which sets in sharply at $\tilde{\varepsilon} := \varepsilon/eV_b = 0.5$. This crossover is shown in figure 3(c) for a selected value of $\gamma_1 = 0.02$. In the following, we will try to fit our measurements to equation (2) in both the low and large ε limit. There are four fitting parameters: ε , Γ_1 , Γ_2^* , and κ . Note that we always use the ansatz $\Gamma_2 = \Gamma_2^* e^{-\kappa d}$ and that we define the zero of the distance axis d to match with the peak position in the measurement. This is possible, as we have no means to determine the ‘true’ zero, i.e. the point of contact of the right electrode with the C₆₀ molecule.

In the first step, we obtain κ by focusing on large d where the junction is widely open and the conductance well below the conductance at the peak. In this simple tunnelling regime, $G \propto \Gamma_2 \propto \varepsilon e^{-\kappa d}$. From fits to the averaged conductance

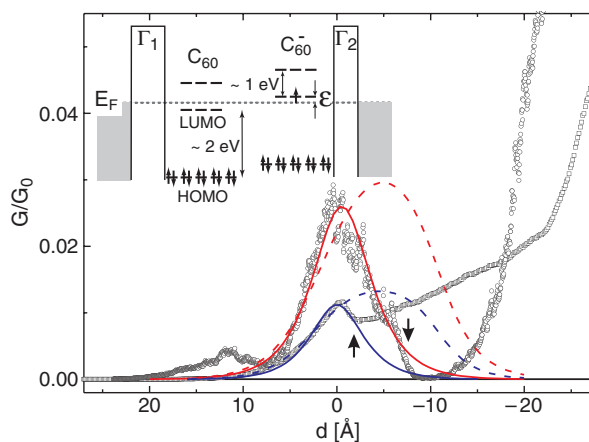


Figure 4. Averaged conductance versus distance curves for DMSO (\square) and toluene (\circ). The solid lines are fits to the data using equation (1) with $\Gamma_1/\varepsilon = 1.1 \times 10^{-2}$ (2.7×10^{-2}) and $\kappa = 0.43 \text{ \AA}^{-1}$ (0.37 \AA^{-1}) for DMSO (toluene). The dashed lines were calculated from equation (2) in the limit $\varepsilon = 0$: $\Gamma_1 = 0.92 \text{ meV}$ (2.2 meV), $\Gamma_2^* = 2.7 \text{ meV}$ (3.9 meV), and $\kappa = 0.43 \text{ \AA}^{-1}$ (0.37 \AA^{-1}) for DMSO (toluene). Inset: Schematic energy diagram of the metal–molecule–metal junction showing the energy level of C_{60} and C_{60}^- . Due to its large electronegativity, C_{60} tends to gain charge from a nearby metallic surface as illustrated by the position of its LUMO level, lying below the Fermi energy of the Au electrodes.

curves of the C_{60} -modified junctions (figure 2 insets), we extract the inverse decay lengths $\kappa_{\text{DMSO}} = 0.43 \pm 0.01 \text{ \AA}^{-1}$ and $\kappa_{\text{toluene}} = 0.37 \pm 0.05 \text{ \AA}^{-1}$. We emphasize that the value obtained for DMSO is more reliable than the one for toluene, since the fit could be performed over a more extended range of conductance. This is due to the presence of a lower conductance peak in toluene (see figure 2(b)). The inverse decay lengths κ are slightly suppressed as compared to the values measured in the solvent alone [21].

We next compare our data to conductance curves calculated in the limit $\varepsilon = 0$. We fix the κ -values to the ones determined for large d and try to obtain a good match with the experiment by tuning both Γ_1 and Γ_2^* . The dashed lines in figure 4 show curves for $\Gamma_{1,\text{DMSO}} = 0.92 \text{ meV}$ and $\Gamma_{2,\text{DMSO}}^* = 2.7 \text{ meV}$, and $\Gamma_{1,\text{toluene}} = 2.2 \text{ meV}$, $\Gamma_{2,\text{toluene}}^* = 3.9 \text{ meV}$. In both cases, the adjusted curves present a substantially broader peak than the data, showing that the limit $\varepsilon = 0$ is inappropriate.

We now relax the condition $\varepsilon = 0$ and try to find the *smallest* possible ε for which a good match between the calculated and measured curve is obtained, again using the κ -values determined for a large d . We obtain $\varepsilon_{\text{DMSO}} \simeq 0.20 \text{ eV}$, $\Gamma_{1,\text{DMSO}} \simeq 4.3 \text{ meV}$, $\Gamma_{2,\text{DMSO}}^* \simeq 0.35 \text{ eV}$, and $\varepsilon_{\text{toluene}} \simeq 0.12 \text{ eV}$, $\Gamma_{1,\text{toluene}} \simeq 5.5 \text{ meV}$, $\Gamma_{2,\text{toluene}}^* \simeq 74 \text{ meV}$. Care has to be taken at this point, because $\varepsilon_{\text{toluene}} \simeq 0.12 \text{ eV}$ is very close to the transition region between the Breit–Wigner and the $\varepsilon = 0$ case where the theoretical $G(d)$ curves are quite sensitive to the temperature. On taking the finite temperature into account, $\varepsilon_{\text{toluene}}$ increases slightly, so $\varepsilon \gtrsim 0.15\text{--}0.2 \text{ eV}$ is a good approximation for both DMSO and toluene.

If we allow for larger values of ε we cross over to the Breit–Wigner equation. In this scale-invariant limit, we obtain convincing fits for both DMSO and toluene with the parameters

$\Gamma_1/\varepsilon = 0.011$ (DMSO) and 0.027 (toluene), and $\Gamma_2^*/\varepsilon = 2$ as required (solid lines in figure 4). Hence, at this stage we can say with confidence that $\varepsilon \gtrsim 0.15\text{--}0.2 \text{ eV}$ for both DMSO and toluene.

As emphasized before, the Breit–Wigner formula cannot provide an upper bound for ε . However, we can—on a physical ground—provide an upper bound on Γ_2 and therefore also on ε . The latter is obtained through the relation $\Gamma_2^* = 2\varepsilon$. The peak in $G(\Gamma_2)$ appears at relatively large Γ_2 -values, but Γ_2 cannot grow to too high values, because otherwise *higher* molecular states of the C_{60} molecule will strongly hybridize with the states in the Au electrode and the model will break down. Moreover, a large Γ_2 at short distances corresponds to a large binding force of order $\kappa\Gamma_2$ between the molecule and the Au electrode. In fact, we think that the crossover from the peak to the plateau in DMSO is determined by this consideration. Furthermore, the fully developed peak in toluene suggests that Γ_2 at the position of the peak (Γ_2^*) is smaller in toluene than in DMSO.

In order to fix the upper bound of Γ_2 we need to discuss the typical energy scales of the orbitals in C_{60} .³ In the inset of figure 4 we show the energy levels of C_{60} and C_{60}^- (adapted from [25]). The HOMO–LUMO gap of C_{60} determined in solution is around 2.3 eV [26] whereas local density approximation calculations provide a value of 1.9 eV for the free C_{60} molecule (see e.g. [15] and references therein). Experiments on C_{60} monolayers assembled on metallic surfaces showed values ranging from 1.5 to 3.0 eV [27–30].

Due to its high electronegativity, a C_{60} molecule in contact with a metal tends to gain charge from the metal. The ionization potential of Au is 5.3 eV and the electron affinity of C_{60} equals 2.8 eV . The latter includes the Coulomb energy of the singly charged C_{60} amounting to $\approx 3 \text{ eV}$. If we assume that the Coulomb energy is strongly screened in the gap between the Au electrodes, $C_{60} \rightarrow C_{60}^-$ is favourable. Photoemission studies of C_{60} on an Au surface yield values for the electron charge on C_{60} of 0.8 [31] and 1.0 [32]. Hence, it is very likely that C_{60} is singly charged also in our work. On acquiring an electron the threefold degenerate LUMO state of C_{60} splits by a very small amount of 8 meV (not shown and also not resolvable in our experiment) and the chemical potential E_F is expected to align closely with this orbital (dashed line). In fact, E_F may lie above ($\varepsilon > 0$) or below ($\varepsilon < 0$), depending on the exact charge state.

Taking the HOMO–LUMO gap of the C_{60} and the C_{60} anion as the proper energy scales, $\Gamma_2 \lesssim 1\text{--}2.3 \text{ eV}$ to avoid hybridization with higher lying orbitals. If we impose that this condition occurs in DMSO at the transition from the peak to the observed plateau at $d = -2 \text{ \AA}$ (see arrow in figure 4), we obtain $\varepsilon_{\text{DMSO}} < 0.2 \dots 0.5 \text{ eV}$. Together with the previous consideration, ε is determined quite accurately to $0.2 < \varepsilon_{\text{DMSO}} < 0.5 \text{ eV}$. Similarly, if we pretend to describe the full peak in toluene up to $d = -7 \text{ \AA}$ (arrow), we obtain $\varepsilon_{\text{toluene}} \lesssim 0.04 \dots 0.09 \text{ eV}$. These rather small values for ε are inconsistent with the previous consideration. In order to obtain an upper bound for $\varepsilon_{\text{toluene}}$ of at least 0.2 eV , one would have to set the cut-off to as large a value as $\Gamma_2 \leq 5 \text{ eV}$. This disagreement shows that the full decay of $G(d)$ in toluene to

³ We do not take into account the modifications in the orbitals induced by the anchor group attached to C_{60} .

approximately zero conductance beyond the peak must have another origin. This will be addressed in the following.

We have assumed here that we are allowed the use the resonant tunnelling model with an unperturbed level beyond the peak. However, a full understanding of the small- d regime would require the understanding of local rearrangement effects taking place when the electrodes and the molecules are reaching mechanical contact. In the case of toluene we observe that the conductance drops to a negligibly small value after the peak and then shows a pronounced increase, similarly to the behaviour of the junction in the pure solvent (figure 2(b)). We can presume that, upon closing of the junction to small values of d , the molecules are pushed away from the inter-electrode space, resulting in conductance properties dominated by Au–Au tunnelling. The shoulder observed in the case of DMSO (figure 2(a)) lets us envision a different scenario in which the molecules remain within the junction and therefore continue to substantially affect the conductance of the junction at very short inter-electrode separations. Additionally, large conductance fluctuations can be observed in toluene (see figure 2(b)) while the curves are much smoother in DMSO. We attribute these differences to the solubility of the fullerene derivative in the solvent considered. Whereas toluene is a good solvent, the fullerenes tend to aggregate with time when suspended in DMSO. In our view, the large conductance fluctuations observed in toluene reflect the tendency of the fullerene molecules to be re-solvated if the cavity becomes too narrow. In contrast, the molecules rather stay within the junction if DMSO is used due to the lower solvation energy.

Whether a single-molecule picture really holds in such a system is an important question. The very good match between theory and experiment supports the single-molecule approach. The analysis provides more than a qualitative agreement with the data and allows the extraction of narrowed range estimates for the LUMO position and the tunnelling rate Γ_1 of the molecular bridge between the Au electrode and the C₆₀ molecule. The results are: $\varepsilon = 0.2 \dots 0.5$ eV, and $\Gamma_1/\varepsilon = 1.1 \dots 2.7 \times 10^{-2}$.

The above discussion is based on a non-interacting model, where the interaction energy has been absorbed in the level energy ε . When the coupling Γ_2 to the molecule changes, the average charge on the molecule is modified, thereby changing the interaction contribution to ε . However, we have numerically checked (within a self-consistent mean-field theory [33]) that this effect does not appreciably change the shape of the conductance versus distance curves, but only slightly scales the parameters ε , Γ_1 and Γ_2^* .

The presence of a much lower peak in some raw conductance curves in toluene (about 12 Å prior to the main peak, figure 2(b)) might be a signature for a weaker tunnelling process involving C₆₀ molecules on both electrodes. If running experiments confirm this feature, an interpretation in terms of a triple-barrier system could further support this approach.

4. Conclusions

We have performed transport measurements through C₆₀ molecules tethered by a single anchor group in Au break junctions operated in a liquid environment. The signature of the presence of the molecules within the junction appeared as

a peak in conductance versus distance curves. The shape of this peak was strongly influenced by the solvent in which the junction was operated, thereby showing the importance of a proper environmental control in nanoscale junctions.

The data can be understood in a resonant tunnelling picture through a single level located close to the Fermi energy E_F . The particular geometry of the experiment combined with the environmental control allowed us to provide numbers for the electronic tunnelling rates between a gold electrode and a fullerene derivative. By systematically varying the linker group, our approach will allow us to better understand the electronic coupling between molecules and electrodes in molecular devices. Moreover, gating will allow the resonant level to be moved even closer to the Fermi level. An increase of the conductance up to the quantum conductance value can then be envisaged.

Acknowledgments

We acknowledge the help of P Morf for reductive desorption measurements. MTG acknowledges a grant from the ‘Ministerio de Educación y Ciencia’. This work benefitted from the support of the Swiss National Center of Competence in Research ‘Nanoscale Science’, the Eurocores Programme on Self-Organized Nano-Structures and the Swiss National Science Foundation.

References

- [1] Park J *et al* 2002 *Nature* **417** 722
- [2] Liang W, Shores M P, Bockrath M, Long J R and Park H 2002 *Nature* **417** 725
- [3] Chen J, Reed M A, Rawlett A M and Tour J M 1999 *Science* **286** 1550
- [4] Collier C P, Wong E W, Belohradský M, Raymo F M, Stoddart J F, Kuekes P J, Williams R S and Heath J R 1999 *Science* **285** 391
- [5] Reed M A, Zhou C, Muller C J, Burgin T P and Tour J M 1997 *Science* **278** 252
- [6] Park H, Lim A K L, Alivisatos A P, Park J and McEuen P L 1999 *Appl. Phys. Lett.* **75** 301
- [7] Cui X D, Primak A, Zarate X, Tomfohr J, Sankey O F, Moore A L, Moore T A, Gust D, Harris G and Lindsay S M 2001 *Science* **294** 571
- [8] Gimzewski J K and Joachim C 1999 *Science* **283** 1683
- [9] Kergueris C, Bourgoin J-P, Palacin S, Esteve D, Urbina C, Magoga M and Joachim C 1999 *Phys. Rev. B* **59** 12505
- [10] Reichert J, Ochs R, Beckmann D, Weber H B, Mayor M and Löhneysen H v 2002 *Phys. Rev. Lett.* **88** 176804
- [11] Champagne A R, Pasupathy A N and Ralph D C 2005 *Nano Lett.* **5** 305
- [12] Krüger M, Buitelaar M R, Nussbaumer T, Schönenberger C and Forró L 2001 *Appl. Phys. Lett.* **78** 1291
- [13] Xiao X Y, Xu B Q and Tao N J 2004 *Nano Lett.* **4** 267
- [14] Jäckel F, Watson M D, Müllen K and Rabel J P 2004 *Phys. Rev. Lett.* **92** 188303
- [15] Dresselhaus M, Dresselhaus G and Eklund P C 1996 *Science of Fullerenes and Nanotubes* (New York: Academic)
- [16] Joachim C and Gimzewski J K 1997 *Chem. Phys. Lett.* **265** 353
- [17] Park H, Park J, Lim A K L, Anderson E H, Alivisatos A P and McEuen P L 2000 *Nature* **407** 57
- [18] Porath D, Levi Y, Tarabiah M and Millo O 1997 *Phys. Rev. B* **56** 9829

- [19] Shi X, Caldwell W B, Chen K and Mirkin C A 1994 *J. Am. Chem. Soc.* **116** 11598
- [20] van Ruitenbeek J M, Alvarez A, Piñeyro I, Grahmann C, Joyez P, Devoret M H, Esteve D and Urbina C 1996 *Rev. Sci. Instrum.* **67** 108
- [21] Grüter L, González M, Huber R, Calame M and Schönenberger C 2005 *Small* at press
- [22] Marcus Y, Smith A L, Korobov M V, Mirakyan A L, Avramenko N V and Stukalin E B 2001 *J. Phys. Chem. B* **105** 2499
- [23] Cui X D, Zarate X, Tomfohr J, Sankey O F, Primak A, Moore A L, Moore T A, Gust D, Harris G and Lindsay S M 2002 *Nanotechnology* **13** 5
- [24] Datta S 1995 *Electronic Transport in Mesoscopic Systems* (Cambridge: Cambridge University Press)
- [25] Green W H Jr, Gorun S M, Fitzgerald G, Fowler P W, Ceulemans A and Titeca B C 1996 *J. Phys. Chem.* **100** 14892
- [26] Echegoyen L and Echegoyen L E 1998 *Acc. Chem. Res.* **31** 593
- [27] Maxwell A J, Brühwiler P A, Nilsson A, Mårtensson N and Rudolf P 1994 *Phys. Rev. B* **49** 10717
- [28] Gensterblum G, Pireaux J J, Thiry P A, Caudano R, Vigneron J P, Lambin Ph, Lucas A A and Krätschmer W 1991 *Phys. Rev. Lett.* **67** 2171
- [29] Wang H, Zeng C, Li Q, Wang B, Yang J, Hou J G and Zhu Q 1999 *Surf. Sci.* **442** L1024
- [30] Lu X, Grobis M, Khoo K H, Louie S G and Crommie M F 2004 *Phys. Rev. B* **70** 115418
- [31] Tzeng C-T, Lo W-S, Yuh J-Y, Chu R-Y and Tsuei K-D 2000 *Phys. Rev. B* **61** 2263
- [32] Hoogenboom B W, Hesper R, Tjeng L H and Sawatzky G A 1998 *Phys. Rev. B* **57** 11939
- [33] Zahid F, Paulsson M and Datta S 2003 *Advanced Semiconductors and Organic Nano-Techniques* ed H Morkoc (New York: Academic)